3D Full Wave Fast Wave Modeling with Realistic Antenna Geometry and SOL Plasma

N. Bertelli[1,a)], S. Shiraiwa[2], G. J. Kramer[1], X. Yang[3], T. DeHaas[3], C. Lau[4], B. Van Compernolle[5], E.-H. Kim[1], J. C. Wright[2] and RF SciDAC Team

[1]*Princeton Plasma Physics Laboratory, Princeton, NJ, USA*
[2]*Plasma Science and Fusion Center, MIT, Cambridge, MA, USA*
[3]*TAE Technologies, Inc., Rancho Santa Margarita, CA, USA*
[4]*Oak Ridge National Laboratory, PO Box 2008, Oak Ridge, TN, USA*
[5]*Department of Physics and Astronomy, University of California, Los Angeles, CA, USA*

[a)]Corresponding author: nbertell@pppl.gov

Abstract. This paper reports the significant advancement of our ability to model and to understand how RF waves interact with the SOL plasma, by simulating the full torus 3D SOL plasma together with the antenna and core plasma. We introduce and use a recently developed and open source code, Petra-M, which was constructed on the scalable MFEM C++ finite element library, and performed 3D full wave simulations in the HHFW regime for both NSTX-U and LAPD plasmas. A first full wave simulation for a full 3D torus including a realistic antenna geometry and SOL plasma region for NSTX-U is presented. A scan of the antenna phasing shows a strong interaction between FWs and the SOL plasma for lower antenna phasing, which is consistent with previous NSTX HHFW observations. The effect of the 3D wave field on the fast ion population from NBI beams in NSTX-U is also discussed by using the 3D field obtained from the Petra-M simulations in the full-orbit following particle SPIRAL code. On LAPD, 3D full wave simulations of a new HHFW 4-strap antenna recently installed by TAE Technologies on LAPD are performed showing a qualitative agreement with experimental data.

INTRODUCTION

In a fusion device powered significantly by RF, the loss of RF power in the scrape-off layer (SOL) can be a real plasma material interface (PMI) issue for possible RF sheaths and plasma facing component damage. Indeed, many experiments in different fast wave (FW) heating regimes, such as hydrogen minority and high harmonic fast wave (HHFW), have found strong interactions between RF waves and the SOL region. Moreover, a significant interaction between FW and energetic ions generated by neutral beam injection (NBI), also, plays an important role in the current experiments. Commonly, RF simulations in the plasma core are neglecting the SOL plasma and they compute the RF field in a 2D domain assuming one single toroidal wave number. Full wave AORSA [1] simulations including the SOL region plasma in 2D geometry with a single toroidal wave number representing the peak of the antenna spectrum have been also performed [2, 3, 4]. State-of-the-art RF SOL/antenna simulation is yet limited to a relatively small volume in front of the antenna, and it involves significant physics simplification such as stratifying antenna strap structure and/or treating the antenna front volume as vacuum. In this paper, instead, the full 3D device geometry is examined including realistic antenna geometry in order to capture the 3D effects and the antenna-plasma interaction in the SOL plasma and, at the same time, the core wave propagation.

This paper is structured as follows: in Section 2, a brief description of the Petra-M code is presented. Numerical applications on NSTX-U and LAPD are discussed in Section 3. Finally, Section 4 contains a brief summary of the work presented here.

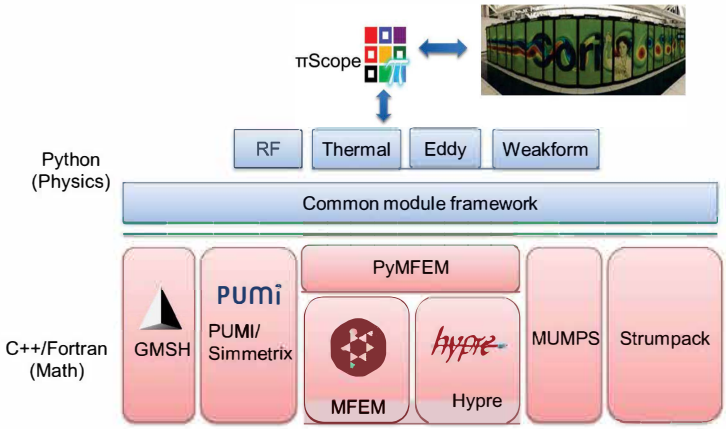

FIGURE 1. Code structure of Petra-M.

BRIEF DESCRIPTION OF Petra-M

Petra-M (Physics Equation Translator for MFEM) is an integrated finite element method (FEM) analysis environment based on MFEM [5]. MFEM is an open source scalable C++ FEM library, developed by Lawrence Livermore National Laboratory team. This library allows to assemble efficiently finite element linear systems for a variety of physics partial differential equations (PDEs) including the Maxwell equations on the computer cluster. Petra-M was previously used for ICRF wave simulations on Alcator C-Mod, which was presented at the last RF conference (22nd Topical Conference on Radiofrequency Power in Plasmas) [6, 7]. However, in order to realize the full torus scale RF simulation for a variety of tokamaks and other devices as discussed here, a significant effort has been made within the RF SciDAC center [8] to improve the capability of Petra-M.

Figure 1 shows the present code structure of Petra-M. The basic code design of handling computationally heavy tasks in a C++/Fortran layer, while providing the physics equation implementation and the user interface using Python, is the same. The parametrized geometry and mesh generation module, which has been used for NSTX-U and LAPD antenna mesh preparation, was added. This module utilizes OpenCASCADE [9] and GMSH [10] Python API. An RF physics interface was also extended to provide the data necessary to transfer the simulation results to the SPIRAL code [11]. We also added the RF Maxwell equations interface for 1D linear and 2D axisymmetric simulations. In terms of the linear solver, we use the new low-rank-approximation feature in the MUMPS solver [12], which reduces the matrix factorization time. Although it is not used in this work yet, we also added an interface to directly specify the finite element linear system equation using the weakform terms, which comes handy when we couple the advanced RF physics model such as the RF rectified potential boundary conditions (BC) [13, 14]. The reader is referred to [15] for more details about Petra-M .

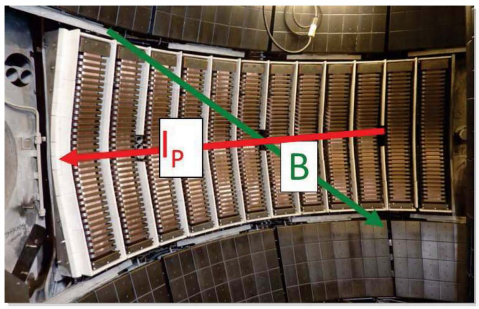

FIGURE 2. (a) NSTX-U HHFW 12-strap antenna. The green and red arrows indicate the magnetic field and plasma current directions, respectively.

NUMERICAL APPLICATIONS

In this Section we present a couple of Petra-M applications: HHFW numerical simulations for the National Spherical Torus eXperiment Upgrade (NSTX-U) and the Large Plasma Device (LAPD) experiments.

NSTX-U

NSTX-U [16, 17] is equipped with the same RF heating system that was present in NSTX. An HHFW 12-strap antenna located on the outboard midplane extending 90 degree toroidally. In Figure 2 the HHFW antenna is shown together with the clockwise direction of the magnetic field (green arrow) and the counter-clockwise direction plasma current (red arrow). One can also note the large magnetic pitch angle, which can be up to 40 degree [4, 18]. Moreover, the antenna phasing adopted generally in the NSTX experiment were 30°, 90°, and 150°, which correspond to a peak of the antenna spectrum, in terms of toroidal wave number, of $n_\phi = 5, 12$, and 21.

Previous HHFW studies of heating efficiency showed large amounts of HHFW power missing from core [18, 19, 20, 21, 22, 23]. In particular, fast camera pictures show bright plasma spirals extending from regions in front of the antenna all the way down to the divertor plasma facing components (PFCs) [18, 20]. Previous modeling indicates that a key important variable causing the FW coupling problem could be the critical SOL plasma density in front of the antenna relative to the FW cutoff density. If the SOL density, n_{SOL}, is larger than the FW cutoff density, the FW fields start to propagate in SOL and begins to fill the SOL region away from the antenna [3]. Examples of modeling efforts for HHFW on NSTX-U [2, 3, 4] show the importance of the SOL density. Recently an approximate scaling of $P_{\mathrm{SOL}} \propto n_{\mathrm{SOL}} V_{\mathrm{SOL}}/(N_{\parallel}^2 B_{\mathrm{T}})$ was obtained for the power loss mechanism [24] (where P_{SOL} is the power absorbed in the SOL region, V_{SOL} is the SOL volume, $N_{\parallel}$ is the parallel refractive index, and B_{T} is the toroidal magnetic field).

In order to be able to run a 3D simulation for NSTX-U plasma we need to generate the 3D solid model for NSTX-U combining the plasma core, the SOL region and the antenna box. Figure 3 shows the antenna mesh obtained within Petra-M by using the GMSH software [10] starting directly from the engineering drawings of the NSTX antenna and the full 3D mesh for the NSTX-U torus including the antenna box with the 12 straps. The full 3D mesh has been obtained rotating toroidally the plasma facing first wall, which is in the EFIT file. The mesh adopted here is uniform.

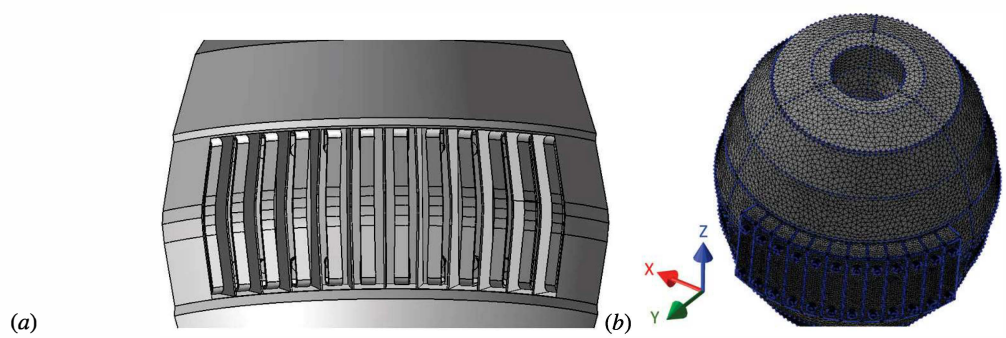

FIGURE 3. (a) NSTX-U HHFW antenna mesh (without Fraday's screens); (b) 3D mesh for NSTX-U plasma incuding the 12-stap antenna box.

The first full 3D torus simulations including realistic antenna geometry obtained by Petra-M are shown in Figure 4. The magnetic equilibrium is obtained from EFIT file for a plasma with $B_T = 1.0$ T was calculated by using the TRANSP code [25]. For these simulations we have assumed vacuum in the antenna box and a magnetized cold plasma with artificial collisions in the torus. The cold plasma model together with collisional damping is indeed a reasonable approximation here since we are interested in the wave electric field just on the antenna structure and surrounding wall and, at the same time, a relatively strong single pass absorption is expected in the scenario analyzed here with broad electron and fast ion absorption profiles (for more details, see [26, 19, 27]). Analytic profiles for the electron density are used with an exponential decay in the SOL plasma with a central density of $n_{e,0} = 5\times10^{19}$ m^{-3} and a density on the last closed flux surface of $n_{e,1} = 5\times10^{18}$ m^{-3} assuming a parabolic profile. Perfect electric conductor (PEC) boundary conditions are used here. Figure 4 shows the E_z component (here z is the vertical direction) of the wave electric field evaluated by Petra-M for three different antenna phasings: 30° (figure (a)), 90° (figure (b)), and 150° (figure (c)). In Figure 4 we show three horizontal planes at $z = -1, 0$, and 1 m in order to show the wave electric field pattern

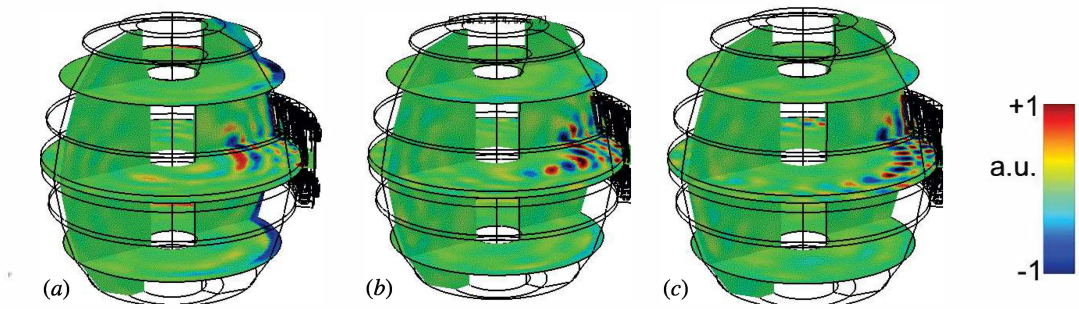

FIGURE 4. E_z component of the wave electric field evaluated by Petra-M for the full 3D NSTX-U torus including the HHFW antenna and three different antenna phasing: 30° (figure (a)), 90° (figure (b)), 150° (figure (c)).

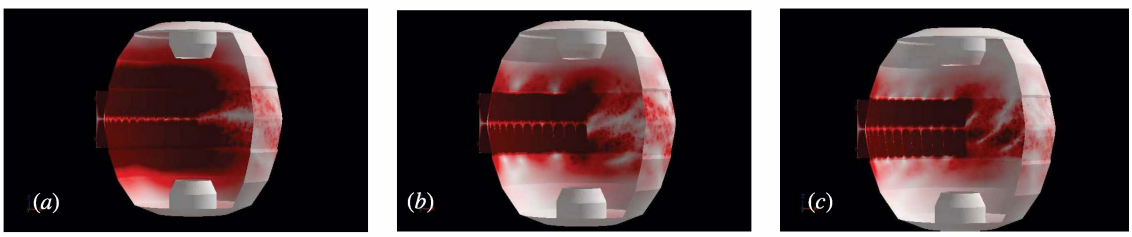

FIGURE 5. Electric field amplitude on the wall surface for three different antenna phasing: 30° (figure (a)), 90° (figure (b)), 150° (figure (c)).

above and below the mid-plane. From figure 4 one can note that: (i) the wave field tends to propagate in the toroidal direction more that the radial direction when the antenna phasing is increased. This is expected because it can be shown analytically that the ratio of the parallel and perpendicular group velocity goes like the parallel refractive index ($N_{\|}$), namely, for higher $N_{\|}$ (or n_ϕ) the waves should travel toroidally more; (ii) some wave field propagation appears in the $z = -1$ m plane both for 30° (figure (a)) and 90° (figure (b)) antenna phasing; (iii) a strong interaction between fast waves and the SOL region occurs for 30° antenna phasing. These results are consistent with the NSTX HHFW observations. Particularly, a qualitative agreement is found between these simulations and an experimental antenna phasing scan done in NSTX and published in [18] (see figure 2 in [18]), where the electron temperature and the stored energy were found to decrease for lower antenna phasing. The 30° antenna phasing was experimentally challenging to have a good HHFW performance in NSTX. This is a combination of two aspects: (i) the strong interaction between fast waves and SOL plasma region (as also shown in figure 4), which is related to the fact that low antenna phasing means low cut-off density ($n_{\text{cut-off}} \propto N_{\|}^2 B\omega$) and (ii) low antenna phasing has also generally a poorer RF heating performance in the core due to the low launched n_ϕ from the antenna. This last point is also shown in [27]. Another additional confirmation of the results described above is shown in figure 5, where the electric field amplitude on the wall surface is shown for the three antenna phasings. From this figure, one can see that very strong electric field on the wall surface appears even far away from the antenna (and even on the center stack although not shown in the figure). The electric field amplitude on the wall surface is higher for lower antenna phasing, in agreement with previous simulations shown in figure 4. For 30° (figure (a)) and 90° (figure (b)) antenna phasing, the antenna corners are particularly critical as shown in different experiments. The electric field on the wall surface in a realistic 3D geometry will be important for studying the antenna impurity generation and RF sheath effects. This will be part of a future work.

Interaction between fast waves and fast ions in NSTX-U

NSTX-U is equipped with two NBI beams (radial and more tangential beams) and up to 10 MW of inject power. From both NSTX experiments and numerical simulations, a strong interaction has been found between HHFW and fast ions generated by NBI [27, 28]. Therefore, it is very important to understand such interaction.

The electric field pattern obtained by Petra-M assuming a cold plasma approximation is a reasonable representa-

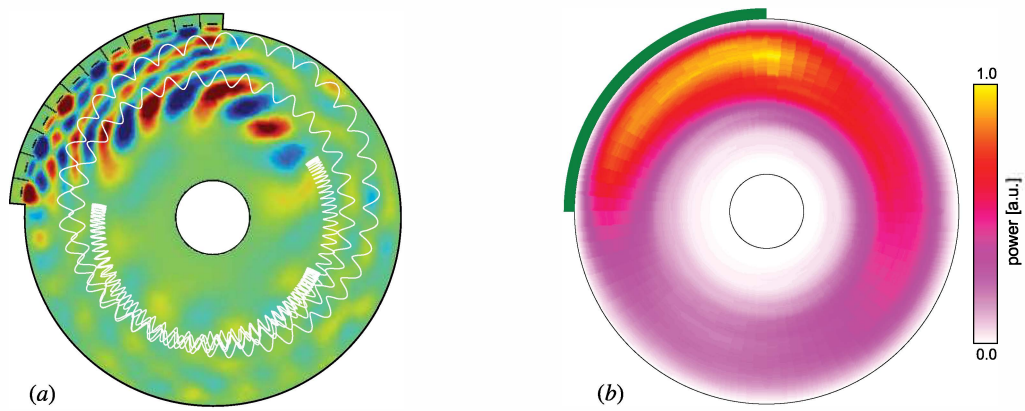

FIGURE 6. (a) E_z component of the wave electric field in the toroidal cross-section (on the mid-plane) with a single fast ion orbit in white; (b) Contour plot of the fast ions power deposition evaluated by SPIRAL including the RF wave field.

tion of the electric field including the kinetic effects mainly due to the fact that in the scenario analyzed here we have a relatively strong single pass absorption and both the Landau and the fast ion dampings are quite broaden (see for more details [26, 19, 27]) allowing the collisional damping used here to replace them reasonably well. Moreover, the region where the wave - fast ion interaction occurs spread broadly, which effectively smears out the impact of detailed difference in wave field amplitude pattern between a cold plasma approximation and the full-hot plasma approximation. For this reason, a logical step is to combine this 3D RF field with the full-orbit following particle code SPIRAL [11] to study the interaction of fast waves with fast ions generated by NBI.

SPIRAL is a full-orbit following test-particle code used to interpret and plan fast-ion experiments in tokamaks. It solves the Lorentz equation taking into account the full gyro orbit effects and, therefore, it captures the interaction between RF heating and fast ions, naturally, which depends on the gyro-motion of the fast ions, by adding the wave electric and magnetic fields to the equilibrium electric and magnetic fields. Figure 6(a) shows the E_z component of the wave electric field in a toroidal cross-section on the mid-plane of NSTX-U overlayed with a single fast ion orbit as obtained by SPIRAL. One can clearly see that the fast ions should be affected mainly in the region in front of the antenna where the wave electric field is strong. In order to show this point we use an ensemble of 40k particles in SPIRAL assuming an initial Maxwellian distribution with a fast ion temperature $T_{\mathrm{fi}} \sim 25$ keV and a central fast ions density of $n_{\mathrm{fi}} \sim 2 \times 10^{18}$ m^{-3}. These parameters of the Maxwellian distribution correspond to the parameters adopted in the full wave simulations performed with AORSA for NSTX-U plasmas [27]. At the same time, we use the three components of the wave electric field evaluated by Petra-M in a 3D geometry as a perturbation of the equilibrium field in the Lorentz equation. The simulation result is shown in figure 6(b) where we show a contour plot of the fast ions power deposition evaluated by SPIRAL including the RF wave field. It clearly appears that the interaction between fast waves and fast ions occurs mainly in front of the antenna, as expected. This result, although expected, demonstrates how 3D effects are important in these simulations for fast ions studies in which RF is included. Generally, a 2D wave field obtained with only a single toroidal wave number is used assuming toroidal symmetry. This approximation results in an acceleration/deceleration of the fast ion due to RF everywhere in the torus and not only in the region where the RF wave field is localized. From figure 6(b), it also appears that the fast ions absorption is mainly located around the 5th deuterium ion cyclotron resonance (the yellow spot in figure 6 (b)), which is the first resonance encountered by the wave electric field. This result is in agreement with the AORSA full wave simulations shown in [27]. Further studies with realistic fast ion distribution functions from the NBI beams in NSTX-U will be investigated in the future.

LAPD

The LArge Plasma Device (LAPD) experiment is a linear machine located in UCLA [29]. It has a cylindrical geometry with reproducible and accessible plasmas. The length of plasma column is about 18 m, a central electron density on the order of 10^{19} m^{-3}, electron temperature of about 10 eV and a magnetic field between 0.1 and 0.25 T. Recently the TAE technologies team in collaboration with the LAPD team has installed and operated a HHFW 4-strap antenna as shown in figure 7. The wave frequency was 10 MHz (although the frequency can be increased up to 35 MHz) with

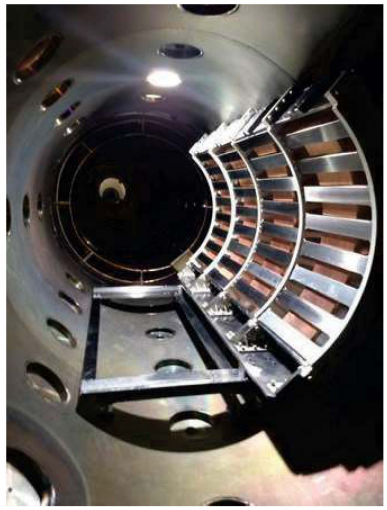

FIGURE 7. HHFW 4-strap antenna implemented in LAPD by TAE technologies.

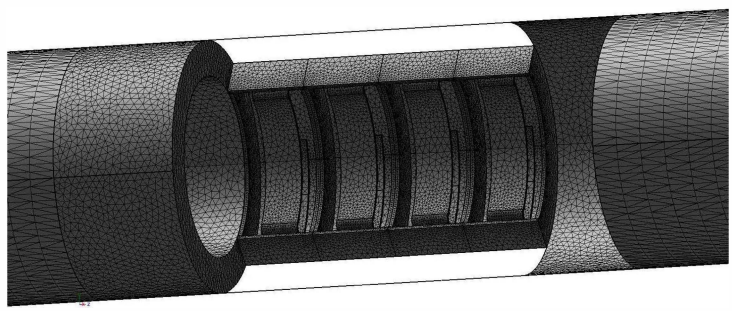

FIGURE 8. 3D mesh for LAPD and the HHFW 4-strap antenna.

five different antenna phasings (30°, 45°, 60°, 90°, and 180°). Moreover, different radial locations of the antenna were considered. The main diagnostics were Langmuir probes, B-dot probes, and emissive probes. More details about the HHFW 4-strap antenna and the RF experimental campaign can be found in [30].

As similarly done for NSTX-U, we first generated a 3D mesh for LAPD including the HHFW 4-strap antenna as shown in figure 8. After that, we assumed a constant magnetic field along the cylinder, $B = 0.1$ T and we assumed a parabolic density profile with central density $n_{e,0} = 2 \times 10^{19}$ m^{-3} and density in front of the antenna $n_{e,1} = 10^{18}$ m^{-3} and vacuum in the antenna box. The B-dot probes measure the magnetic wave field components which can be compared directly to the numerical simulations. Indeed, in LAPD we can have very high quality and high resolution measurements of the wave electric and magnetic fields due to its reproducible and accessible plasmas and the probe drive system (in both the poloidal and horizontal planes) can collect high resolution data at thousands of points in a few hours [31, 32].

Figure 9 shows the first 3D result obtained by Petra-M for the HHFW 4-strap antenna implemented in LAPD. This figure shows the B_z component of the wave magnetic field on a horizontal plane at $y = 0$ and two poloidal cross-sections in the middle of the two outer straps. In this simulation we assume 180° antenna phasing and the antenna mouth is located at $R \sim -25$ cm, here R is the distance between antenna and machine axis. Figure 10 shows a comparison between the B_z in the poloidal cross-section evaluated by Petra-M and the measured one by the B-dot probes. The yellow square in figure 10(a) indicates roughly the measurement plane. A qualitative agreement is obtained. In particular, one can note the similar wave field pattern in the core of the cylinder. Further improvements in the numerical simulations are being made to the antenna mesh, the mesh resolution and reduce the numerical domain,

the use of the experimental electron density profile.

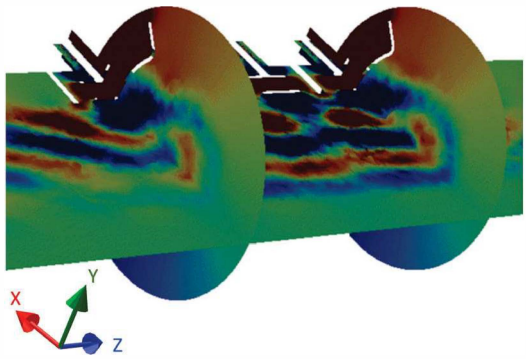

FIGURE 9. B_z component of the wave magnetic field evaluated by Petra-M for the full 3D LAPD experiment including the HHFW 4-strap antenna.

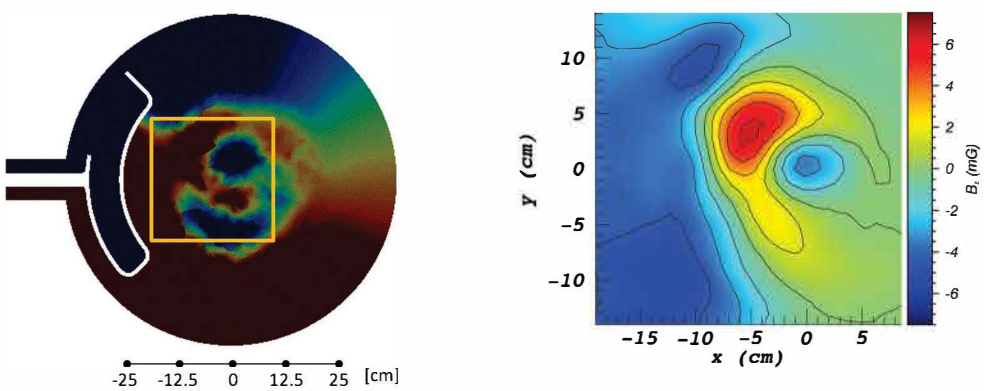

FIGURE 10. Simulated (figure (a)) and measured (figure (b)) B_z component of the wave magnetic field in the poloidal cross-section. In figure (a) the yellow square represents the measurement plane as a reference.

CONCLUSIONS

We have showed the first full wave simulation for a full 3D torus including a realistic antenna geometry for NSTX-U plasma assuming a cold plasma dielectric tensor with an artificial collisions. An antenna phasing scan was performed showing a very strong interactions between fast waves and SOL plasma region for low antenna phasing consistent with NSTX experimental data. A first attempt to couple the 3D RF solver with the full-orbit following particle code SPIRAL was presented showing that the 3D effects can play an important role in the interaction between RF and fast ions. However, in this first attempt we used a cold plasma model with collisions for the core propagation. Although the wave propagation and absorption characteristic permits to use the cold plasma with collisions as a reasonable first order approximation, its accuracy remains being investigated in detail with a model including the kinetic effects. In fact, we plan in the future to model the core and the edge plasma with the full wave code TORIC and Petra-M, respectively, in order to take into account the kinetic effects as previously done in ICRF H-minority heating scenario in C-Mod [6]. Finally, an initial comparison between Parta-M simulation for a HHFW 4-strap antenna mounted on LAPD and its RF wave field measurements for LAPD plasma was also presented and discussed showing a qualitative

agreement in the magnetic wave field pattern. As a future steps, we are planning to (i) improve the 3D NSTX-U plasma and antenna meshes; (ii) study the effects of RF on fast ions in NSTX-U for both the "old" and the new more tangential NBI beams; (iii) further investigate the slow wave in front of the antenna including the RF rectified potential boundary conditions; (iv) perform 3D simulations for the ITER-like antenna in JET and stellarator configurations where the 3D effects play a dominant role.

ACKNOWLEDGMENTS

The first author N. B. would like to thank Dr. M. Ono for useful discussions. This work was supported by a U.S. Department of Energy (DOE) Scientific Discovery through Advanced Computing Initiative Contract Number DE-SC0018090 and the U.S. DOE under DE-AC02-CH0911466. In addition, this research used resources of the National Energy Research Scientific Computing Center (NERSC), a U.S. Department of Energy Office of Science User Facility operated under Contract No. DE-AC02-05CH11231.

REFERENCES

1. E. F. Jaeger and et al, Phys. Plasmas **8**, p. 1573 (2001).
2. D. L. Green and et al, Phys. Rev. Lett. **107**, p. 145001 (2011).
3. N. Bertelli and et al, Nucl. Fusion **54**, p. 083004 (2014).
4. N. Bertelli and et al, Nucl. Fusion **56**, p. 016019 (2016).
5. MFEM, (http://mfem.org).
6. J. C. Wright and S. Shiraiwa, EPJ Web of Conferences **157**, p. 02011 (2017).
7. S. Shiraiwa and et al, EPJ Web of Conferences **157**, p. 03048 (2017).
8. Center for Integrated Simulation of Fusion Relevant RF Actuators, (https://sites.google.com/view/rfscidac4/).
9. OpenCASCADE, (https://www.opencascade.com/).
10. GMSH, (http://gmsh.info).
11. G. J. Kramer and et al, Plasma Phys. Control. Fusion **55**, p. 025013 (2013).
12. MUMPS: a parallel sparse direct solver, (http://mumps.enseeiht.fr/).
13. J. R. Myra and D. A. D'Ippolito, Phys. Plasmas **22**, p. 062507 (2015).
14. H. Kohno and et al, Phys. Plasmas **22**, p. 072504 (2015).
15. S. Shiraiwa and et al, to be submitted to Nucl. Fusion (2019).
16. J. E. Menard and et al, Nucl. Fusion **52**, p. 083015 (2012).
17. J. E. Menard and et al, Nucl. Fusion **57**, p. 102006 (2017).
18. J. C. Hosea and et al, Phys. Plasmas **15**, p. 056104 (2008).
19. C. K. Phillips and et al, Nucl. Fusion **49**, p. 075015 (2009).
20. R. J. Perkins and et al, Phys. Rev. Lett. **109**, p. 045001 (2012).
21. R. J. Perkins and et al, Nucl. Fusion **53**, p. 083025 (2013).
22. R. J. Perkins and et al, Phys. Plasmas **22**, p. 042506 (2015).
23. R. J. Perkins and et al, Nucl. Materials and Energy **12**, p. 283 (2017).
24. E.-H. Kim and et al, Phys. Plasmas **26**, p. 062501 (2019).
25. S. P. Gerhardt, R. Andre, and J. E. Menard, Nucl. Fusion **52**, p. 083020 (2012).
26. M. Ono, Phys. Plasmas **2**, p. 4075 (1995).
27. N. Bertelli and et al, Nucl. Fusion **59**, p. 086006 (2019).
28. N. Bertelli and et al, AIP Conf. Proc. **1580**, p. 310 (2014).
29. W. Gekelman and et al, Rev. Sci. Instrum. **87**, p. 025105 (2016).
30. X. Yang and et al, "Overview of tae's hhfw project on lapd," in *23rd Topical Conference on Radiofrequency Power in Plasmas*, to be published in AIP Conf. Proc. (2019).
31. B. Van Compernolle and et al, "Fast wave experiments on lapd in support of fusion," in *23rd Topical Conference on Radiofrequency Power in Plasmas*, to be published in AIP Conf. Proc. (2019).
32. G. Bal and et al, "Rf sheath rectification near antennas with metallic and insulating side walls," in *23rd Topical Conference on Radiofrequency Power in Plasmas*, to be published in AIP Conf. Proc. (2019).